Biochemistry and Biophysics Reports 40 (2024) 101838

Contents lists available at ScienceDirect

Biochemistry and Biophysics Reports

journal homepage: www.elsevier.com/locate/bbrep

Comparison of two-dimensional and three-dimensional culture systems and their responses to chemotherapy in cells representing disease progression of high-grade serous ovarian cancer

Naya El Mokbel [a], Alicia A. Goyeneche [a], Rewati Prakash [a], Benjamin N. Forgie [a], Farah H. Abdalbari [a], Xing Zeng [b], Basile Tessier-Cloutier [a], Shuk On Annie Leung [b,c,1,*], Carlos M. Telleria [a,c,1,**]

[a] McGill University, Experimental Pathology Unit, Department of Pathology, Faculty of Medicine and Health Sciences, Montreal, QC, Canada
[b] McGill University Health Centre, Division of Gynecologic Oncology, Department of Obstetrics and Gynecology, Montreal, QC, Canada
[c] Research Institute of the McGill University Health Centre, Cancer Research Program, Montreal, QC, Canada

ARTICLE INFO

Keywords:
Ultra-low attachment
Anchorage-free
3D culture
2D culture
High grade serous ovarian cancer
Anticancer drugs
Multicellular tumor spheroids

ABSTRACT

High-grade serous cancer is the most common type of ovarian cancer and is usually diagnosed at advanced stages with high mortality due to recurrence and eventual resistance to standard platinum therapy. The aim of this study was to compare two-dimensional (2D) versus tridimensional (3D) cell culture as a preclinical model of response to carboplatin, paclitaxel and niraparib using PEO1, PEO4 and PEO6 cell lines, which were generated from the same patient along disease progression. Morphologically, cells formed flat adherent layers versus spheroidal structures with different compaction patterns in 2D and 3D respectively. In 2D, apoptosis was rare whereas in 3D cells formed a multilayered structure with an outer layer of live proliferating cells and an inner core of apoptotic cells. Furthermore, a differential capacity to produce ATP was observed among the cell lines in 3D but not in 2D. While response to carboplatin, paclitaxel and niraparib in both settings followed a similar trend, a lower sensitivity was observed in 3D with respect to 2D. Overall, 3D cell culture is likely more reflective of the *in vivo* cellular tumor behavior and more suitable of therapeutic evaluation given its added complexity absent in 2D.

1. Introduction

Ovarian cancer is the fourth most common gynecologic cancer and is associated with a high mortality rate [1]. High grade serous ovarian cancer (HGSOC) is the most common histological subtype that is usually diagnosed at advanced stages and accounts for the highest mortality [2]. Platinum-based therapy has been the cornerstone of treatment with introduction of PARP inhibitors as maintenance therapy, especially for patients with homologous recombination deficiencies such as *BRCA* mutations [3]. In predicting therapeutic response, preclinical models that recapitulate the complexity of *in vivo* tumors are needed. The commonly used 2D cell culture model is economical but is simplified and may not mimic essential *in vivo* cellular organization and interactions. Cells in anchorage-free 3D culture model mimics *in vivo* poor vascularized conditions, in which the multilayered structure and their nutrients, pH, and oxygen concentration gradients, offer a complex preclinical model for *in vitro* experiments that bridges the gap between 2D cell culture and animal models for drug testing [4–11]. The multicellular tumor spheroid (MCTS) model consists of cancer cells in a single suspension that are prevented to adhere to a substrate and that grow with fetal bovine serum and without adding extracellular matrix (ECM) [12]. The aim of this study was to compare the biological and morphological

* Corresponding author. McGill University Health Centre, Division of Gynecologic Oncology, Department of Obstetrics and Gynecology, Montreal, QC, Canada.
** Corresponding author. McGill University, Experimental Pathology Unit, Department of Pathology, Faculty of Medicine and Health Sciences, Montreal, QC, Canada.
E-mail addresses: naya.elmokbel@mail.mcgill.ca (N. El Mokbel), alicia.goyeneche@affiliate.mcgill.ca (A.A. Goyeneche), rewati.prakash@mail.mcgill.ca (R. Prakash), benjamin.forgie@mail.mcgill.ca (B.N. Forgie), farah.abdalbari@mail.mcgill.ca (F.H. Abdalbari), xing.zeng@mcgill.ca (X. Zeng), basile.tessiercloutier@mcgill.ca (B. Tessier-Cloutier), annie.leung@mcgill.ca (S.O. Annie Leung), carlos.telleria@mcgill.ca (C.M. Telleria).
[1] Both the authors contributed equally.

https://doi.org/10.1016/j.bbrep.2024.101838
Received 12 July 2024; Received in revised form 24 September 2024; Accepted 2 October 2024

adaptation of HGSOC cell lines along the disease progression grown on a 3D environment with respect to morphology, viability, and drug response, and contrasted with the 2D adaptation. These HGSOC cell lines were developed from the same patient offering unique features acquired during disease advancement.

2. Material and methods

2.1. Cell lines

PEO1 were generated after response to first diagnosis post platinum-based therapy when the patient was still platinum sensitive, PEO4 were obtained after first recurrence when platinum resistance was already manifested, whereas PEO6 were obtained prior to the death of the patient just a few months after obtaining PEO4 [13]. All cells were derived from a single patient with HGSOC (kindly provided by Dr. Taniguchi, University of Washington, USA) [14,15]. A schematic showing the timeline of cell line development was elegantly published in 2010 [15]. PEO1 have been found to be mutant for *BRCA2* while PEO4 and PEO6 have a reversal mutation that reconstitutes the *BRCA2* wild-type status [14]. All cell lines were authenticated using autosomal short tandem repeat (STR) profiling markers showing a $\geq$80 % match between the cells used in this study. The SRT authentication profile was recently published in a manuscript from our laboratory [16].

2.2. Culture environment

Flat-bottom T75 flasks (Thermo Fisher Scientific, Rochester, NY, USA) and 96-well plates (Corning Incorporated, Kennebunk, ME, USA) were used in 2D. For 3D, 96-well transparent (Corning Incorporated, Kennebunk, ME, USA) or white (S-BIO, Hudson, NH, USA) ultra-low attachment round-bottom plates (ULAPs) were used to facilitate spheroidal formation [17]. Cells were maintained in RPMI 1640 medium (Gibco, Grand Island, NY, USA) prepared in HyPure cell culture grade water (Cytiva, Logan, UT, USA) and supplemented with 10 mM HEPES (Corning), 10 mL penicillin (Corning), 200 mM glutamine (Glutamax, Corning), 10 μg/mL insulin (Gibco), 10 mL sodium pyruvate (Corning), 5 % fetal bovine serum (Corning), 5 % bovine serum (Corning) and 23.8 mM sodium bicarbonate (Millipore Sigma, St. Louis, MO, USA) at a constant temperature of 37 °C in a humidified atmosphere of 5 % CO_2. Media was changed every 48–72 h when cells were cultured in flat-bottom T75 flasks. For morphological analysis, cells were plated in cell culture-treated flat-bottom T75 flasks for 2D while 5000 cells/well were plated in ULAPs for 3D. For the Live/Dead, apoptosis, proliferation, and drug testing experiments, 5000 cells/well were plated in flat-bottom plates and ULAPs for 2D and 3D respectively. For the ATP quantitation assay, 10000 and 5000 cells/well were plated for 2D and 3D respectively to maximize cell adhesion during the 24-h incubation period in flat-bottom plates. For the Live/Dead assay positive controls, PEO1, PEO4 and PEO6 cells were plated with 5000 cells/well for 2D culture while PEO6 cells were plated with 5000 cells/well for 3D culture. For the apoptosis detection assay positive control in 2D, PEO1 and PEO4 cells were plated with 5000 cells/well.

2.3. Morphological analysis

The morphology of the cells in flat-bottom flasks was assessed at one and five days for PEO1 and PEO4 which is enough time for the cells to stablish a representative adherent component, while two and seven days for PEO6 is required to establish its adherent phenotype. Cell arrangement in ULAPs was assessed at one, four and seven days for compaction level defined as the average cross-sectional area of three wells per cell line determined using ToupView Software (OMAX, USA). A decrease in average cross-sectional area with time represented an increase in compactness.

2.4. Cell viability assay

The viability of the cells was assessed using the Live/Dead cell assay. After four days in the plates for 2D culture and four and seven days for 3D culture, Calcein-AM (live cells indicator), EthD-1 (dead cells indicator) (Live/Dead Viability/Cytotoxicity Kit, Thermo Fisher Scientific, Eugene, OR, USA), and the NucBlue™ ReadyProbes™ reagent (nuclei indicator) (Thermo Fisher Scientific, Eugene, OR, USA) were added to the cells followed by imaging. For the positive control, the cells were fixed with a 4 % PFA solution on day four before undergoing the Live/Dead assay to facilitate penetration of the non-permeable dead cells indicator and disruption of the esterase activity indicator of cell viability.

2.5. Apoptosis detection assay

The method of cell death was assessed using a CellEvent™ Caspase-3/7 assay. After three days in the plates for 2D and three and six days for 3D, the CellEvent™ Caspase-3/7 Green ReadyProbes™ reagent (Thermo Fisher Scientific) was added to the cells. 24 h later, caspase-3/7 activation was assessed and NucBlue™ ReadyProbes™ reagent was added for nuclei detection. Since we have found recently that the gold complex auranofin [18] causes apoptosis in PEO1 and PEO4 cells [19], a positive control in which the two cell lines were exposed to the drug was included. PEO1 and PEO4 cells were plated in three groups: caspase-3/7 and DMSO (Corning) (vehicle group), caspase-3/7, DMSO and auranofin 2 μM, and caspase-3/7, DMSO and auranofin 4 μM.

2.6. Proliferation detection assay

The Click-iT EdU cell proliferation assay (Click-iT EdU Alexa Fluor 594 Imaging Kit, Thermo Fisher Scientific), which assesses the incorporation of a fluorescently labeled mimetic of the thymidine nucleotide, EdU, into newly synthesized DNA to indicate cells with ongoing DNA synthesis, was used to assess proliferation. After three days in the plates for 2D culture and three and six days for 3D culture, 10 μM of EdU dissolved in DMSO were added to the cells [16]. 24 h later, the Click-iT solution containing an EdU reaction buffer, copper (III) sulfate, the Alexa Fluor 594 azide dye and a Click-iT EdU buffer additive as well as Hoechst (nuclei indicator) were added to the cells followed by imaging.

2.7. ATP quantitation assay

The CellTiter-Glo luminescent and 3D cell viability assays (Promega Corporation, Madison, WI, USA) were used. After 24 h in the flat-bottom plate and four and seven days in the ULAPs, the CellTiter-Glo reagent was added to the cells followed by shaking on an orbital shaker and finally plate reading. A negative control for the CellTiter-Glo assays was included by adding the CellTiter-Glo reagent to three wells without cells.

2.8. Drug testing

Drug response was assessed using the CellTiter-Glo luminescent and 3D cell viability assays as described above. After four days in the ULAPs, the cells were exposed to carboplatin (25 μM, 50 μM, 100 μM or 200 μM), paclitaxel (1.25 μM, 2.5 μM, 5 μM or 10 μM) or the PARP inhibitor niraparib (2 μM, 4 μM, 8 μM or 16 μM). Cell lines were kept for four days, point of maximal compaction, in the plates before drug exposure. The concentrations of the drugs utilized comprised lower and higher concentrations than the Cmax values recommended for *in vitro* studies, 135 μM for carboplatin and 4.27 μM for paclitaxel [20]. Since no data was available for niraparib, the Cmax of olaparib, 13.1 μM, was used instead.

2.9. Statistical analysis

Experiments were done with three to seven replicates for each cell

line in each experiment; experiments were repeated twice with similar outcome. Analysis for the ATP quantitation assays results was performed using one-way ANOVA followed by the Tukey's multiple comparison test. For the cross-sectional areas and drug testing results analysis, we performed two-way ANOVA followed by the Dunnett's multiple comparison test. For the CellEvent™ Caspase-3/7 and Click-iT EdU Cell Proliferation assay results, statistical analysis was performed using unpaired *t*-test.

2.10. Plate imaging and reading parameters

BioTek Cytation3 Imaging Reader and Gen5 software were used for fluorescent and luminescent plate imaging. For the Live/Dead assay, the excitation and emission values were set as follows: green 494 nm and 516 nm, red 528 nm and 617 nm, and blue 359 nm and 461 nm. For the apoptosis detection assay, the excitation and emission values were set as follows: green 502 nm and 530 nm, blue 359 nm and 461 nm. For the cell proliferation detection assay, the excitation and emission values were set as follows: red 590 nm and 615 nm, blue 359 nm and 461 nm.

3. Results

3.1. Morphology

In 2D culture, all cells formed monolayers and islands of uniform polygonal cells (Fig. 1a) [13]. PEO1 had an elongated shape whereas PEO4 and PEO6 tended to grow on top of each other. In ULAP, all cell lines formed 3D spheroidal structures which became more compacted (decrease in average cross-sectional area) from day one to four (Fig. 1b–s1). From day four to seven, compaction remained stable in PEO1 while PEO4 and PEO6 reached maximum compactness at day four and became less compacted at day seven. At days four and seven, the average cross-sectional area of PEO1 was smaller than that of PEO4 which was smaller than that of PEO6 (Fig.s1).

3.2. Cell viability

In 2D, cells displayed a homogeneous and flat green viable culture with minimal red cell toxicity (Fig. 2a). On Fig. s4 and Fig. s5 cells on 2D and 3D respectively were fixed allowing the non-permeable

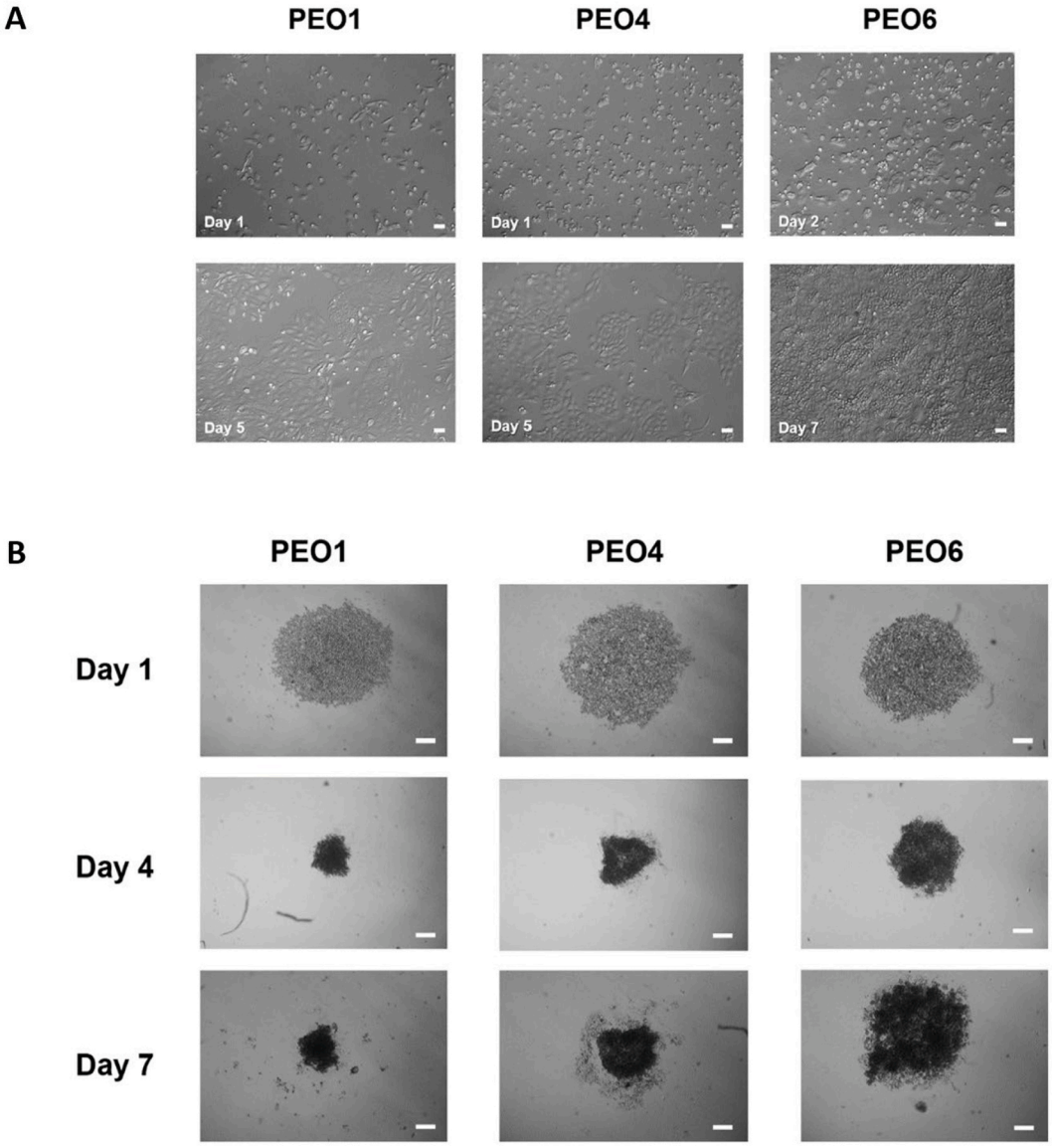

Fig. 1. Morphology in 2D cultures and 3D cultures. A) PEO1 and PEO4 cells at days one and five and PEO6 cells at days two and seven in flat-bottom T75 flasks. Scale bars = 50 μm. B) PEO1, PEO4 and PEO6 cells at days one, four, and seven in ULAPs. Scale bars = 200 μm.

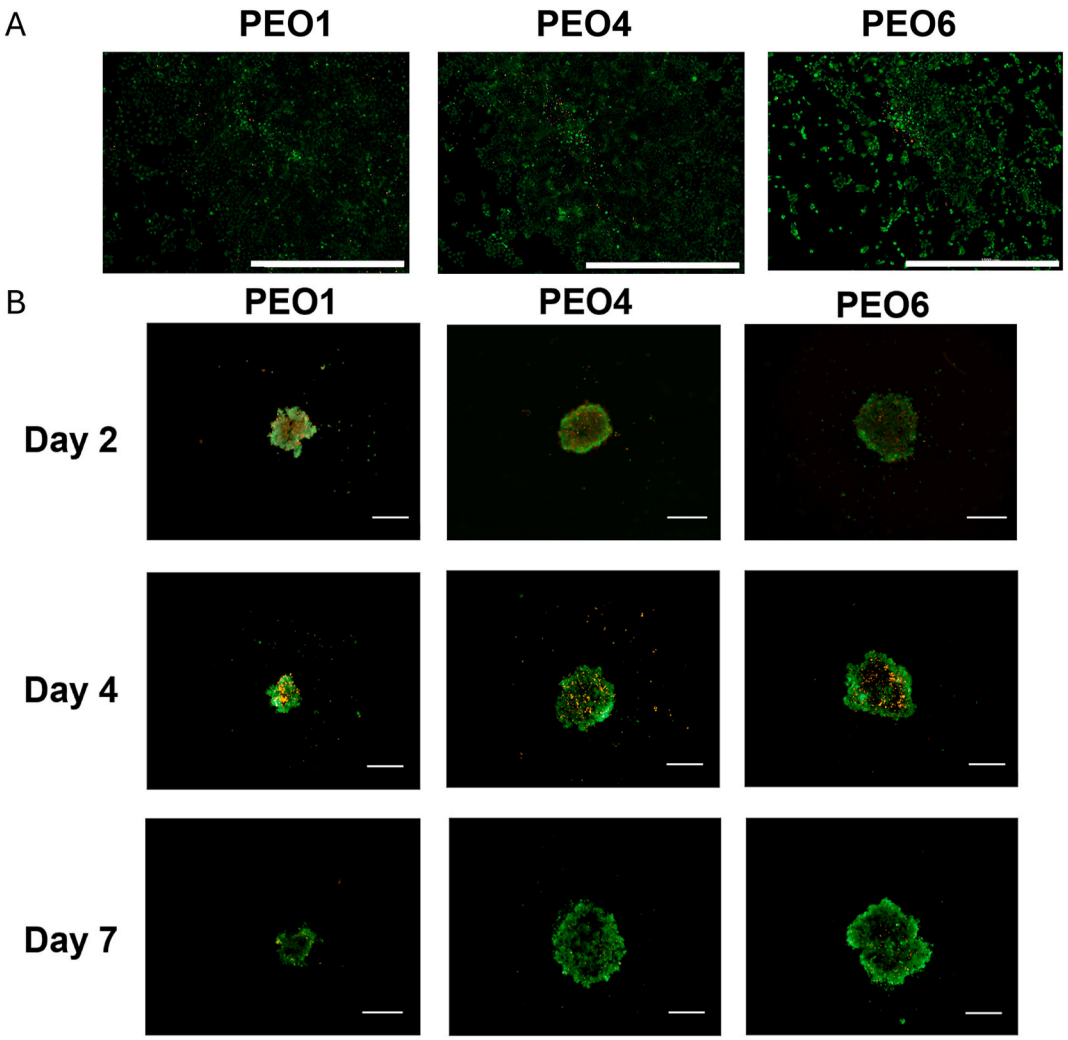

Fig. 2. Viability in 2D cultures and 3D cultures. A) Live (Green)/Dead (Red) images at day four in flat-bottom plates. Scale = 1000 μm. B) Live (Green)/Dead (Red) at days two, four, and seven in ULAPs. Scale bars = 500 μm. (For interpretation of the references to colour in this figure legend, the reader is referred to the Web version of this article.)

fluorochrome to enter the cells and demonstrating the positive control of the dead fluorochrome indicator. In 3D, cells displayed an outer layer of live cells at the periphery of the spheroidal structures and an inner layer of dead cells in the center, but at different time points (Fig. 2b–s3). Two days after plating, the structures of PEO1, PEO4, and PEO6 had few dead cells. Four days after plating, the structures had an almost fully developed core of dead cells mainly for PEO1 and PEO4 which developed a more compact spheroid, while at seven days after plating, the structures had no visible dead cells in the center. The spheroidal structures of PEO6 had few dead cells at day four, and at day seven after plating, the structures had an empty whole in the center. Calcein-AM (live cells) and EthD-1 (dead cells) fluorescence units graphs show that from two to seven days after plating, PEO1 had a decrease in the levels of live and dead cells while PEO4 had no significant change in the levels of live cells but had a decrease in the levels of dead cells (Fig.s2). Across the three time-points, PEO6 had no significant change in the levels of live and dead cells. In summary PEO1 and PEO4 had a slight decrease in cell viability at day four but did not went further on day seven when compared to day two, while cell death seems to decrease at day seven but with an empty core.

3.3. Apoptosis detection

In 2D, only a few apoptotic cells were scattered randomly on the bottom of the plates across all cell lines (Fig. 3a). In 3D, PEO1 apoptotic cell death was confined to the center of the spheroidal structures at day four and seven, while PEO4 and PEO6 cell death occurs in the center of the spheroidal structures at day four and was spread all over the spheroidal structures at day seven (Fig. 3b). Green fluorescence relative units indicate that PEO1 apoptosis levels decreased from day four to seven but did not change significantly during the same time for PEO4 and PEO6 (Fig. 3b) A positive control to test the caspase 3/7 reagent is provided in Fig. s6.

3.4. DNA synthesis pattern reflective of cell proliferation

In 2D, DNA synthesis in PEO1, PEO4 and PEO6 across the plates' surface was detected as indicated by the purple fluorescence (i.e., a superposition of red and blue) (Fig. 3c). The percentages of positive nuclear EdU indicate that DNA synthesis levels in 2D of PEO1 were higher than those of PEO4 and PEO6, reaching statistical significance only with PEO4 (Fig. 3c). In 3D culture, the three cell lines were found to proliferate mostly in the outer layer of the cellular structures (Fig. 3d). Averaging relative red fluorescence units indicate that the DNA synthesis level of all three cell lines did not change significantly from day four to seven (Fig. 3d).

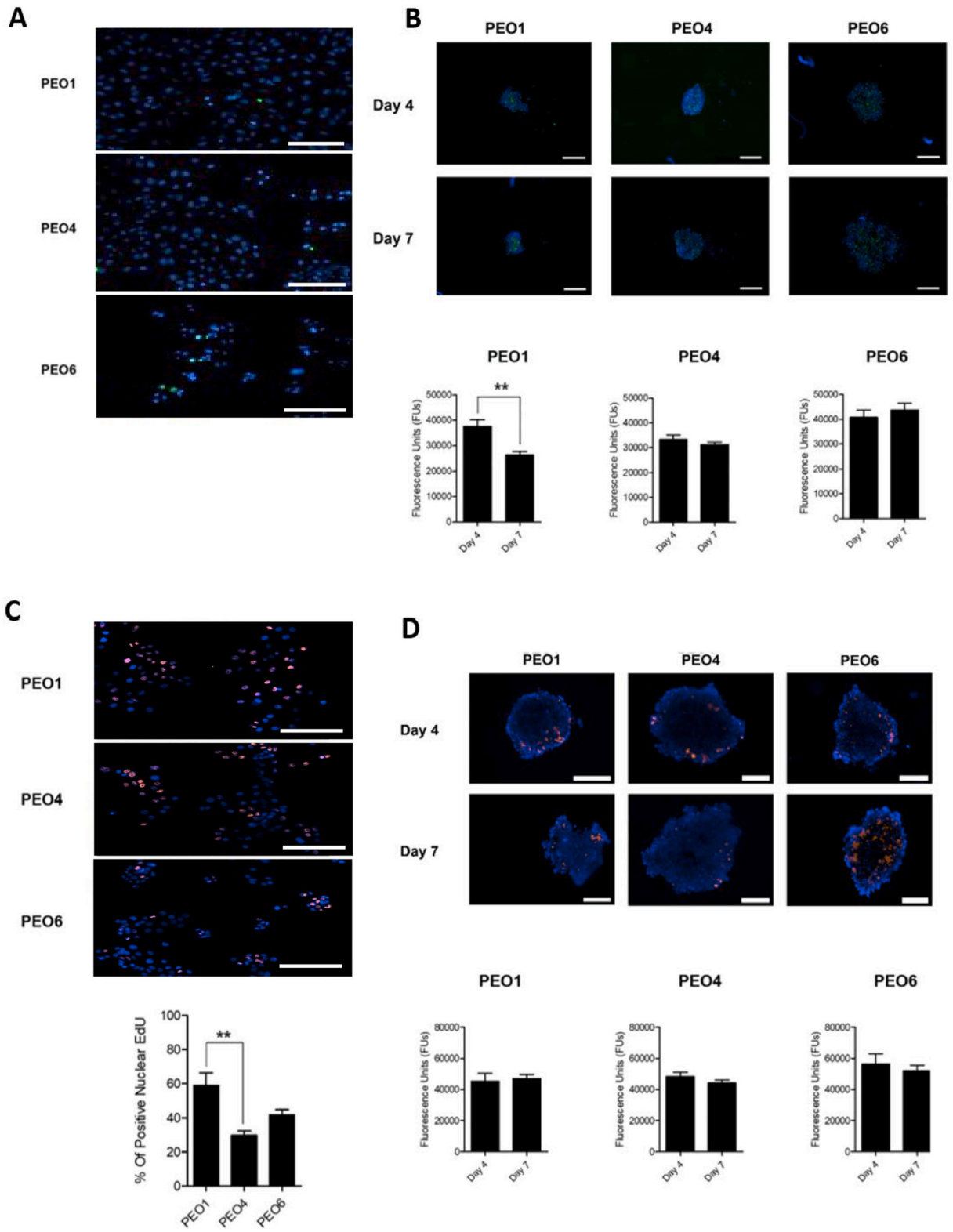

Fig. 3. Cell death and proliferation in 2D cultures and 3D cultures. A) Green and blue indicate apoptosis and nuclear staining respectively. Scale bars = 125 μm. B) The graphs represent the Caspase-3/7 activation in green fluorescence units. **p < 0.01. Scale bars = 500 μm. C) Red and blue indicate proliferation and nuclear staining respectively and purple is the superposition of red and blue. The percentages of positive nuclear EdU indicative of DNA synthesis levels four days after plating are shown in the graph. ** means p < 0.01. Scale bars = 125 μm. D) The graphs represent the cell proliferation assay; red fluorescence units results are indicative of proliferation levels. Scale bars = 200 μm. (For interpretation of the references to colour in this figure legend, the reader is referred to the Web version of this article.)

3.5. Metabolic activity

In 2D, the three cell lines produced levels of ATP that differed slightly from each other with PEO6 producing a higher amount of ATP followed by PEO1 and then PEO4 24 h after plating (Fig. 4a). In 3D, at days four and seven, it was found that PEO6 produced approximately four times more ATP than PEO4 followed by PEO1 that produced approximately eight times less ATP than PEO6 (Fig. 4b).

3.6. Drug testing

In 2D, all four concentrations of carboplatin reduced ATP levels in a concentration-dependent manner in PEO1 cells while only 100 μM and 200 μM caused a decrease of ATP in PEO4 cells (Fig. 4c). The production of ATP in PEO6 cells increased at 25 μM and 50 μM of carboplatin with no effect at 100 μM and decreased only at 200 μM. The ATP levels in all three cell lines were found to be reduced by paclitaxel to a similar extent at the four concentrations used. Only 4 μM, 8 μM and 16 μM of niraparib caused a decrease in ATP levels in PEO1 cells while none of the concentrations had a significant effect on PEO4 and PEO6 cells. In 3D, the ATP production in PEO1 and PEO4 decreased when exposed to carboplatin in a concentration-dependent manner, although to a lesser extent in PEO4 reflecting their platinum resistance (Fig. 4c). The production of ATP in 3D PEO6 cells increased at 25 μM, 50 μM and 100 μM of carboplatin with no effect at 200 μM, indicating that the cells from advanced disease become more resistant and that the adaptation to anchorage-free environment illustrates better this intrinsic behavior. The levels of ATP in all three cell lines were found to be reduced by paclitaxel to a similar extent at the four concentrations used. Only 8 μM and 16 μM of niraparib caused a decrease in ATP levels in PEO1 cells while none of the concentrations had a significant effect on PEO4 and PEO6 cells, supporting that these serial cells lines retained the resistance

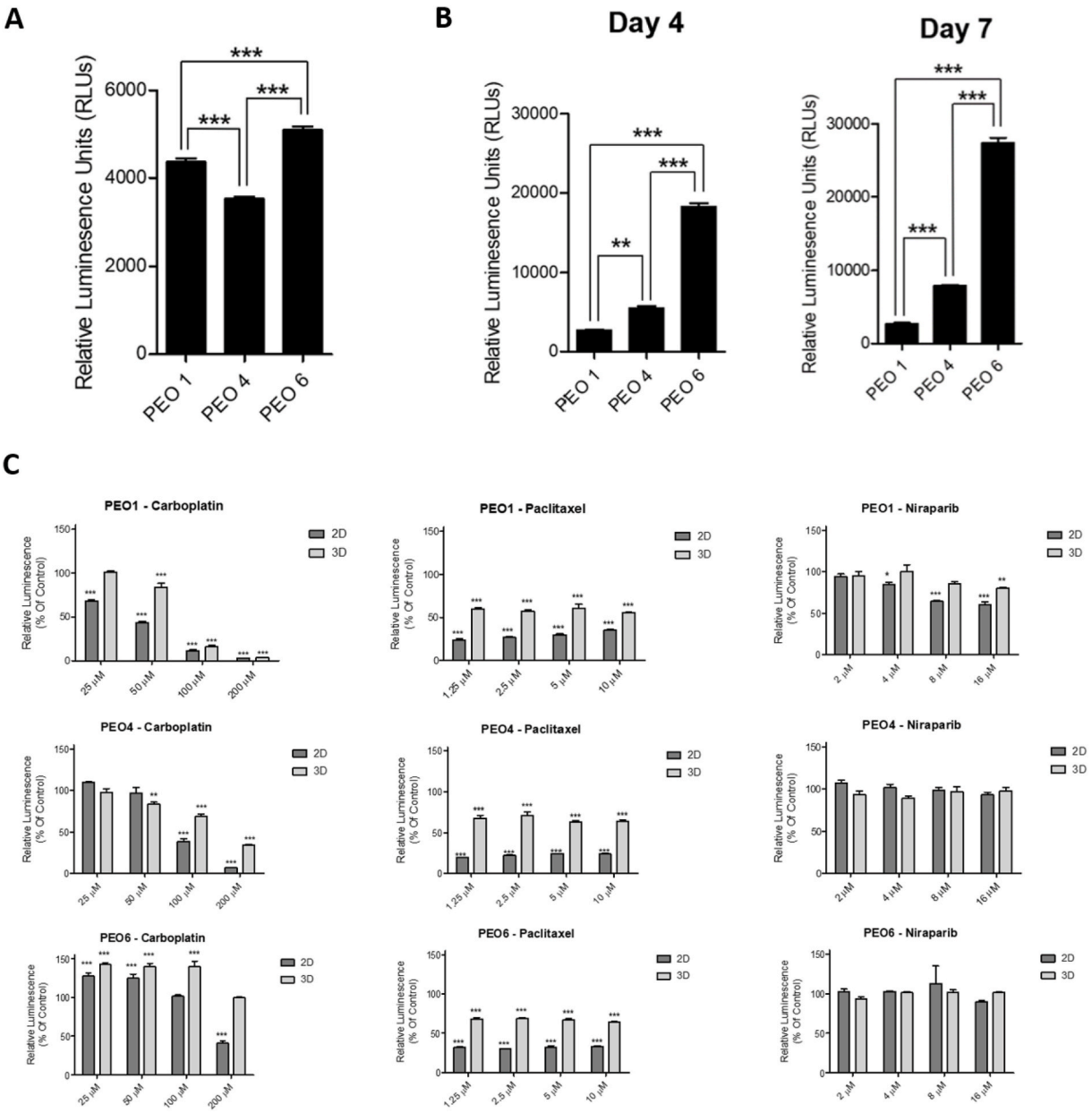

Fig. 4. Metabolic activity and drug response in 2D cultures and 3D cultures. A) ATP production levels on 2D 24 h after plating. B) ATP production levels on 3D four and seven days after plating. ** means $p < 0.01$ and *** means $p < 0.001$. C) Drug response to carboplatin, paclitaxel and niraparib through ATP production levels on 2D and 3D contrasted to 100 % of vehicle. *$p < 0.05$, **$p < 0.01$, ***$p < 0.001$.

acquired *in vivo* during disease advancement. When the drug had an impact on cellular ATP production, it was found to be less effective in 3D than in 2D.

4. Discussion

This study compared cellular adaptation on 3D anchorage-free environment of HGSOC cell lines from the same patient at different times during disease evolution and different *BRCA* statuses and contrasted to regular 2D environment. The behavior of PEO1, PEO4 and PEO6 cells, in terms of morphology, viability, metabolic activity, and drug response, demonstrated greater complexity in 3D culture compared to a more uniform response in 2D culture. Consistent with previous literature, drug response in flat- and round-bottom plates followed a similar trend with lower sensitivity to the drugs observed in the 3D culture setting. For instance, Lee et al. compared the biological and molecular features of 31 epithelial ovarian cancer cell lines with 2D cultures and primary tumors and found that the cells were more chemoresistant in 3D compared with 2D culture [21]. Furthermore, Muguruma et al. investigated differences in drug sensitivities between 2D and 3D culture systems in triple-negative breast cancer cell lines and found that cells were more chemoresistant in 3D than 2D [22].

While no specific pattern of live and apoptotic cells was observed in 2D, cells within the spheroids formed in 3D culture had different levels of viability and death associated with their proliferative capacity and apoptotic state. In general, live proliferating cells were present at the periphery while apoptotic cells accumulated in the center. Such behavior correlates with findings in previous studies that highlight the similarity of such pattern to the cellular behavior of *in vivo* tumors as limited nutrients and agents penetration in the center generates a healthy outer layer of cells with high proliferative ability and a hypoxic dead core [6,23]. The observed decrease in drug sensitivity in 3D could thus be attributed to the reduced access of chemotherapy agents to internal cells in the un-vascularized 3D spheroids due to their structure characterized by a metabolite density gradient [8,22,24,25].

In this study, the effect of carboplatin observed in PEO1 (platinum-sensitive) and PEO4 (platinum-resistant) in 2D and 3D culture correlated with the cell lines' platinum sensitivity described [15,16]. The effect of paclitaxel on the three cell lines was stronger in 2D than 3D, independent of the concentrations used. Considering that PEO1 is mutant for *BRCA2* while PEO4 and PEO6 carry a *BRCA2* reversion, the result that niraparib had an effect on PEO1 but not PEO4 and PEO6 reinforces that the cell lines used are good models to study for drug response [15,26]. Moreover, the fact that PEO4 and PEO6 did not respond to niraparib in both 2D, and 3D suggests that when cells do not respond to a drug, the lack of response will be apparent in both models. Therefore, when designing drug screening experiments while being cautious of the technique used, it would be useful to evaluate the cells' drug response in 2D culture first since it is a simpler and more economical model to use than 3D. If the cells respond to the drug, the response can be confirmed with more concordance with the *in vivo* response using the 3D model [27].

For PEO1, PEO4 and PEO6, the spheroidal structures became more compact from day one to four. From day four to seven, PEO1 had a decrease in apoptosis and viability without significant change in proliferation levels nor average cross-sectional area of the spheroidal structures, suggesting a stagnant level of compaction. While PEO4 and PEO6 had no significant change in their apoptosis and proliferation levels from day four to seven, the average cross-sectional area increased during this period, suggesting a decrease in the level of compaction. These results suggest that the three cell lines reached a common maximum level of compaction at day four. Consequently, day four was selected as the day to expose the cells to drugs as this was the time of maximal morphological stability and thus results would likely be more reproducible.

ATP production levels of cells in a flat-bottom plate in which they adhere to the bottom were also measured and presented as luminescence levels to determine the intrinsic ATP production of the three cell lines when in 2D. PEO1, PEO4 and PEO6 did have the ability to produce ATP in flat-bottom plates with similar biologically relevant levels compared to in 3D. In 3D culture, a differential capacity of the cells to produce ATP was observed with PEO6 producing a four times higher amount of ATP followed by PEO4 and then PEO1 four and seven days after plating. Such differential capacity might reflect the *in vivo* cellular adaptation based on the disease state that PEO6 represent. High ATP levels are a key driver of aggressive cancer cell phenotypes. ATP-high cancer cells show increases in many aggressive properties or behaviors, including anchorage-independence, metastasis and antioxidant capacity [28]. Therefore, the ability of PEO6 to produce significantly higher levels of ATP than the other two cell lines in 3D culture could be linked to an increase in mitochondrial mass and to the aggressive disease state that it represents [28].

The lack of tumor stroma is a significant limitation of this study as tumor stroma is a crucial component mediating drug response and tumor cell behavior [29,30]. Thus, experiments like ours should be contrasted against either presence of extracellular matrix proteins, co-cultures of ovarian cancer cells with cells representing the tumor microenvironment, or within the complexity of ovarian organoids maintained in culture [31].

Given that PEO1 had a more visible and pronounced apoptotic core than PEO4 and PEO6 in 3D, taken together with morphology, Live/Dead assay, apoptosis detection and ATP quantitation, this suggests that as cells become more compacted, those in the center have less access to necessary components of the media leading to lower metabolic activity and apoptotic cell death. Such results suggest that the 3D culture environment provides a level of complexity absent in 2D culture making it more reflective of the *in vivo* cellular tumor behavior central to assessment of therapeutic responses. As HGSOC is the most aggressive ovarian cancer subtype and generally presents at an advanced stage with poor long-term survival, developing *in vitro* models that are as faithful as possible to the *in vivo* tumor behavior to accurately determine therapeutic efficacy of treatments, and thus, potentially increase patient survival is of vital importance.

CRediT authorship contribution statement

Naya El Mokbel: Writing – review & editing, Writing – original draft, Visualization, Validation, Methodology, Investigation, Formal analysis, Conceptualization. **Alicia A. Goyeneche:** Writing – review & editing, Writing – original draft, Visualization, Validation, Supervision, Project administration, Methodology, Investigation, Formal analysis, Conceptualization. **Rewati Prakash:** Writing – review & editing, Software, Investigation. **Benjamin N. Forgie:** Writing – review & editing, Software, Investigation, Formal analysis. **Farah H. Abdalbari:** Writing – review & editing, Investigation. **Xing Zeng:** Writing – review & editing, Supervision, Conceptualization. **Basile Tessier-Cloutier:** Writing – review & editing, Supervision, Conceptualization. **Shuk On Annie Leung:** Writing – review & editing, Writing – original draft, Visualization, Validation, Supervision, Resources, Project administration, Methodology, Investigation, Funding acquisition, Formal analysis, Conceptualization. **Carlos M. Telleria:** Writing – review & editing, Writing – original draft, Visualization, Validation, Supervision, Resources, Project administration, Methodology, Funding acquisition, Conceptualization.

Declaration of competing interest

The authors declare that they have no known competing financial interests or personal relationships that could have appeared to influence the work reported in this paper.

Data availability

Data will be made available on request.

Acknowledgements

This work was supported by the Graduate Excellence Award from the Department of Pathology of McGill University and the Research Institute of the McGill University Health Center Studentship Award.

Appendix B. Supplementary data

Supplementary data to this article can be found online at https://doi.org/10.1016/j.bbrep.2024.101838.

References

[1] Z. Momenimovahed, A. Tiznobaik, S. Taheri, H. Salehiniya, Ovarian cancer in the world: epidemiology and risk factors, Int J Womens Health 11 (2019) 287–299.
[2] N. Anzar, M.R. Hasan, M. Akram, N. Yadav, J. Narang, Systematic and validated techniques for the detection of ovarian cancer emphasizing the electro-analytical approach, Process Biochem. 94 (2020) 126–135.
[3] M.T. Adolphsen J, G. Martin, Z. Mahmoudjafari, R. Meier, W. Shae, D.C. Koestler, C. Bohnenkamp, Duration of response to PARP inhibitors for maintenance treatment of ovarian cancer in patients with germline or somatic HRD, J Hematol Oncol Pharm 13 (2023) 192–198.
[4] S. Gunti, A.T.K. Hoke, K.P. Vu, N.R. London Jr., Organoid and spheroid tumor models: techniques and applications, Cancers (2021) 13.
[5] V. Heredia-Soto, A. Redondo, A. Berjon, M. Miguel-Martin, E. Diaz, R. Crespo, A. Hernandez, L. Yebenes, A. Gallego, J. Feliu, D. Hardisson, M. Mendiola, High-throughput 3-dimensional culture of epithelial ovarian cancer cells as preclinical model of disease, Oncotarget 9 (2018) 21893–21903.
[6] M. Millard, I. Yakavets, V. Zorin, A. Kulmukhamedova, S. Marchal, L. Bezdetnaya, Drug delivery to solid tumors: the predictive value of the multicellular tumor spheroid model for nanomedicine screening, Int. J. Nanomed. 12 (2017) 7993–8007.
[7] P. Sainz-Arnal, I. Pla-Palacín, N. Sánchez-Romero, M. Almeida, S. Morini, E. Solanas, A. Lue, T. Serrano-Aulló, P.M. Baptista, Chapter 62 - bioengineering of liver tissue, in: A. Atala, R. Lanza, A.G. Mikos, R. Nerem (Eds.), Principles of Regenerative Medicine, third ed., Academic Press, Boston, 2019, pp. 1101–1113.
[8] S. Melissaridou, E. Wiechec, M. Magan, M.V. Jain, M.K. Chung, L. Farnebo, K. Roberg, The effect of 2D and 3D cell cultures on treatment response, EMT profile and stem cell features in head and neck cancer, Cancer Cell Int. 19 (2019) 16.
[9] J. Yang, S. Huang, S. Cheng, Y. Jin, N. Zhang, Y. Wang, Application of ovarian cancer organoids in precision medicine: key challenges and current opportunities, Front. Cell Dev. Biol. 9 (2021) 701429.
[10] R.M. Sutherland, Cell and environment interactions in tumor microregions: the multicell spheroid model, Science 240 (1988) 177–184.
[11] Spheroids in cancer research, Methods and perspectives, recent results, Cancer Res. 95 (1984) 1–183.
[12] L.B. Weiswald, D. Bellet, V. Dangles-Marie, Spherical cancer models in tumor biology, Neoplasia 17 (2015) 1–15.
[13] S.P. Langdon, S.S. Lawrie, F.G. Hay, M.M. Hawkes, A. McDonald, I.P. Hayward, D. J. Schol, J. Hilgers, R.C. Leonard, J.F. Smyth, Characterization and properties of nine human ovarian adenocarcinoma cell lines, Cancer Res. 48 (1988) 6166–6172.
[14] W. Sakai, E.M. Swisher, C. Jacquemont, K.V. Chandramohan, F.J. Couch, S. P. Langdon, K. Wurz, J. Higgins, E. Villegas, T. Taniguchi, Functional restoration of BRCA2 protein by secondary BRCA2 mutations in BRCA2-mutated ovarian carcinoma, Cancer Res. 69 (2009) 6381–6386.
[15] S.L. Cooke, C.K. Ng, N. Melnyk, M.J. Garcia, T. Hardcastle, J. Temple, S. Langdon, D. Huntsman, J.D. Brenton, Genomic analysis of genetic heterogeneity and evolution in high-grade serous ovarian carcinoma, Oncogene 29 (2010) 4905–4913.
[16] A. Goyeneche, M.A. Lisio, L. Fu, R. Srinivasan, J. Valdez Capuccino, Z.H. Gao, C. Telleria, The capacity of high-grade serous ovarian cancer cells to form multicellular structures spontaneously along disease progression correlates with their orthotopic tumorigenicity in immunosuppressed mice, Cancers 12 (2020).
[17] E. Tomas, T.G. Shepherd, Insights into high-grade serous carcinoma pathobiology using three-dimensional culture model systems, J. Ovarian Res. 16 (2023) 70.
[18] F.H. Abdalbari, C.M. Telleria, The gold complex auranofin: new perspectives for cancer therapy, Discov Oncol 12 (2021) 42.
[19] F.H. Abdalbari, E. Martinez-Jaramillo, B.N. Forgie, E. Tran, E. Zorychta, A. A. Goyeneche, S. Sabri, C.M. Telleria, Auranofin induces lethality driven by reactive oxygen species in high-grade serous ovarian cancer cells, Cancers (2023) 15.
[20] D.R. Liston, M. Davis, Clinically relevant concentrations of anticancer drugs: a guide for nonclinical studies, Clin. Cancer Res. 23 (2017) 3489–3498.
[21] J.M. Lee, P. Mhawech-Fauceglia, N. Lee, L.C. Parsanian, Y.G. Lin, S.A. Gayther, K. Lawrenson, A three-dimensional microenvironment alters protein expression and chemosensitivity of epithelial ovarian cancer cells in vitro, Lab. Invest. 93 (2013) 528–542.
[22] M. Muguruma, S. Teraoka, K. Miyahara, A. Ueda, M. Asaoka, M. Okazaki, T. Kawate, M. Kuroda, Y. Miyagi, T. Ishikawa, Differences in drug sensitivity between two-dimensional and three-dimensional culture systems in triple-negative breast cancer cell lines, Biochem. Biophys. Res. Commun. 533 (2020) 268–274.
[23] A.G. Mitrakas, A. Tsolou, S. Didaskalou, L. Karkaletsou, C. Efstathiou, E. Eftalitsidis, K. Marmanis, M. Koffa, Applications and advances of multicellular tumor spheroids: challenges in their development and analysis, Int. J. Mol. Sci. 24 (2023) 6949.
[24] A. Ciucci, M. Buttarelli, A. Fagotti, G. Scambia, D. Gallo, Preclinical models of epithelial ovarian cancer: practical considerations and challenges for a meaningful application, Cell. Mol. Life Sci. 79 (2022) 364.
[25] C. Jensen, Y. Teng, Is it time to start transitioning from 2D to 3D cell culture? Front. Mol. Biosci. 7 (2020) 33.
[26] K. Moore, N. Colombo, G. Scambia, B.G. Kim, A. Oaknin, M. Friedlander, A. Lisyanskaya, A. Floquet, A. Leary, G.S. Sonke, C. Gourley, S. Banerjee, A. Oza, A. Gonzalez-Martin, C. Aghajanian, W. Bradley, C. Mathews, J. Liu, E.S. Lowe, R. Bloomfield, P. DiSilvestro, Maintenance olaparib in patients with newly diagnosed advanced ovarian cancer, N. Engl. J. Med. 379 (2018) 2495–2505.
[27] M.N. Brodeur, K. Simeone, K. Leclerc-Deslauniers, H. Fleury, E. Carmona, D. M. Provencher, A.M. Mes-Masson, Carboplatin response in preclinical models for ovarian cancer: comparison of 2D monolayers, spheroids, ex vivo tumors and in vivo models, Sci. Rep. 11 (2021) 18183.
[28] M. Fiorillo, B. Ozsvari, F. Sotgia, M.P. Lisanti, High ATP production fuels cancer drug resistance and metastasis: implications for mitochondrial ATP depletion therapy, Front. Oncol. 11 (2021) 740720.
[29] I. Yakavets, S. Jenard, A. Francois, Y. Maklygina, V. Loschenov, H.P. Lassalle, G. Dolivet, L. Bezdetnaya, Stroma-rich Co-culture multicellular tumor spheroids as a tool for photoactive drugs screening, J. Clin. Med. 8 (2019).
[30] B.D. Landry, T. Leete, R. Richards, P. Cruz-Gordillo, H.R. Schwartz, M. E. Honeywell, G. Ren, A.D. Schwartz, S.R. Peyton, M.J. Lee, Tumor-stroma interactions differentially alter drug sensitivity based on the origin of stromal cells, Mol. Syst. Biol. 14 (2018) e8322.
[31] O. Kopper, C.J. de Witte, K. Lohmussaar, J.E. Valle-Inclan, N. Hami, L. Kester, A. V. Balgobind, J. Korving, N. Proost, H. Begthel, L.M. van Wijk, S.A. Revilla, R. Theeuwsen, M. van de Ven, M.J. van Roosmalen, B. Ponsioen, V.W.H. Ho, B. G. Neel, T. Bosse, K.N. Gaarenstroom, H. Vrieling, M.P.G. Vreeswijk, P.J. van Diest, P.O. Witteveen, T. Jonges, J.L. Bos, A. van Oudenaarden, R.P. Zweemer, H.J. G. Snippert, W.P. Kloosterman, H. Clevers, An organoid platform for ovarian cancer captures intra- and interpatient heterogeneity, Nat. Med. 25 (2019) 838–849.